Egyptian Journal of Chemistry

http://ejchem.journals.ekb.eg/

Synthesis and Evaluation of Corrosion Inhibitor Based on Copolymeric Modified Chitosan Core-Shell Nanocomposite

B. S. Elewa [a*], E. A. Fouad [b], W. I. Eldougdoug [c], M. M. El-Desouky [d]

[a, b, d] *Department of Basic Engineering Sciences, Banha Faculty of Engineering, Banha University, Egypt.*
[c] *Chemistry Department, Faculty of Science, Banha University, Egypt..*

Abstract

A new aqueous dispersible nanocomposite as a green semi-synthetic polymer corrosion inhibitor was developed by a free radical copolymerization of o-aminophenol with anthranilic acid in presence of chitosan (CH/poly-OAP-co-AA). The developed inhibitor performance was tested by surface scanning and electrochemical analysis in aqueous HCl (0.1 M). Using (SEM) scanning electron microscope, (TEM) transmission electron microscope and (FTIR) Fourier transform infrared, the chemical composition and surface properties of CH/poly-OAP-co-AA and morphology of treated steel were explored. The outcomes of performance experiments display very impressive results as corrosion inhibitor, the effectiveness of the inhibition grew as the quantity of the newly synthesised inhibitor rose. Langmuir isotherm was detected to be the most suitable to represent chemisorption of CH/poly-OAP-co-AA on steel surface.

Keywords: o-Aminophenol; Anthranilic acid; Copolymerization; Chitosan; Steel; Potentiodynamic polarization; Chemisorption.

1. Introduction

Corrosion, the metal deterioration caused by chemical or electrochemical processes within the immediate environment, poses a significant challenge to industries worldwide. In particular, acidic mediums play a crucial role in accelerating the corrosion process, causing severe damage and economic losses. Consequently, extensive research has been conducted to develop effective corrosion protection strategies that are both environmentally friendly and economically viable [1].

This study focuses on investigating the potential of a new formulation formed of three corrosion inhibitors "anthranilic acid, amino phenol, and chitosan" for protecting metals against corrosion in acidic mediums. Due to these inhibitors' innate qualities, such as their great stability, low toxicity, and availability from natural sources, attention has been drawn to them. By examining their performance as corrosion inhibitors, this research aims to provide valuable insights into their practical application and effectiveness in real-world scenarios [1].

Anthranilic acid, also known as o-aminobenzoic acid, is a versatile compound that has been extensively studied for its diverse applications. It possesses a functional carboxylic acid group (-COOH) with an amino unit (-NH2), which enables it to interact with metal surfaces through chemisorption and form a protective barrier against corrosive

agents. Numerous studies have reported the excellent inhibitory properties of anthranilic acid, particularly in acidic environments [2-4].

Amino phenol, a class of organic compounds containing both amino and phenolic groups, has also shown promise as a corrosion inhibitor. The presence of these functional groups allows amino phenols to form complexes with metal ions, effectively hindering electrochemical reactions responsible for corrosion. Several studies have highlighted the remarkable efficiency of amino phenols in preventing corrosion in various metal systems [5,6].

Chitosan, produced by deacetylation of chitin, is an organic polymer abundantly witnessed in the exoskeletons of aquatic organisms. Attention has been drawn to this biodegradable and non-toxic material as a possible corrosion inhibitor because of its film-forming ability and strong adhesion to metal surfaces. Chitosan has exhibited excellent inhibitory effects in alkaline, acidic and neutral environments [7-12].

To assess the performance of these inhibitors, a range of experimental techniques will be employed. (EIS) electrochemical impedance spectroscopy will be utilized to monitor the alterations in the electrochemical actions of the metallic substances when the compounds that inhibit are present. EIS measures the impedance response of the system, providing information about the corrosion rate,

_____

_____

polarization resistance, and capacitance. Potentiodynamic polarization will be employed to evaluate the corrosion potential and current of corrosion of the metal, enabling determination of the inhibition efficiency [13-17]. Using surface exterior (SEM) and interior (TEM) analysis, will be performed to explore the morphology and composition of new synthesized copolymeric modified chitosan core-shell nanocomposite and the metal surfaces before and after exposure to the corrosive mediums.

The findings of this study will assist with the growth of effective corrosion protection strategies in acidic mediums. By evaluating the corrosion inhibition performance of the new formulation, this study aims to provide practical insights and recommendations for industrial applications. Furthermore, understanding the mechanisms of corrosion inhibition by these inhibitors will facilitate the optimization of their concentrations and application methods, enhancing their efficiency and durability in real-world conditions.

2.   Experimental
2. 1.   Materials

o-Aminophenol, Anthranilic acid, Chitosan (average molecular weight of 160000 g/mol), hydrous ferrous sulphate and Ammonium peroxydisulphate (APS) were purchased from (Merk, India) with purity higher than 98 %. Hydrochloric acid (30 – 34) % and Acetic acid 98 % was commercial grade from El-NASR Co.

2. 2.   Instrumentation

Potentiostatic and polarization systems (PGZ 100, Volta Master 4 software) were utilized for the introductory tests of anticorrosive features. These experiments were achieved by a triple chamber with platinum counter electrode, mild steel bar like working electrode and saturated calomel electrode serving like reference electrode.

The mild steel employed to be the working electrode was manufactured with an exposure area of 1 cm^2, and the potential was scanned from -0.6 to 0.6 Volts at a scan rate of 10 mVS^{-1}, followed by being submerged in a separate hydrochloric acid sample.

The experimentation involved scratching metal surfaces with sheets of varying grades (1200–2000), degreasing them with AR–grade acetone, rinsing them with deionized water, and then placing them in the test solution.

By extrapolating Tafel curves, variables like (Ecorr) corrosion potential and (Icorr) corrosion current density have been established .

FT/IR-BRUKER, Vector 22 (Germany) Spectrophotometer was utilized for measuring IR spectra for produced nanocomposites. It was feasible to investigate how surfaces are shaped of the produced nanocomposite and steel surface utilising SEM. Microanalyzer microscope (QUANTA 250 SEG, HOLANDA) has been employed for collecting the micrographs. (TEM) (E/M) (JEOL [JEM-1230 electron microscope) has been employed to measure the nanocomposite's manufactured particle size.

2. 3.   Synthesis of nano composites

Through using desired weight ratio of Chitosan (3%) and free radical polymerization homogenous nanocomposites of CH/poly-AA and CH/poly-OAP have been produced. The desired nanocomposite CH/poly-OAP-co-AA was developed using the same weight ratio of chitosan. Then I$_{corr}$ and E$_{corr}$ found in CH/poly-AA, CH/poly-OAP and CH/poly-OAP-co-AA polarization graphs were compared.
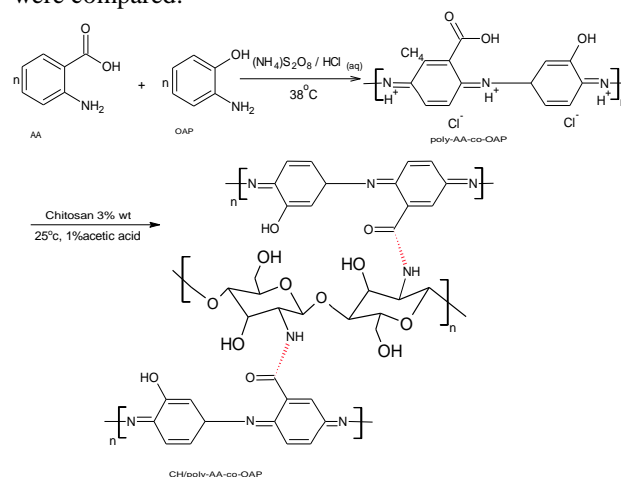
Scheme 1: Copolymerization of AA with OPA and synthesis of CH/poly-OAP-co-AA.

Procedure of Synthesizing nano CH/poly-AA, CH/poly-OAP and CH/poly-OAP-co-AA

By merging Chitosan particles through radical, free polymerization of AA and/or OAP in the presence of APS as a redox initiator, CH/poly-AA, CH/poly-OAP and CH/poly-OAP-co-AA was developed. Generally, 50 ml / 0.3 N HCl solution was utilized to disperse 1mmol of monomer (0.137 g of AA and/or 0.1085 g OAP) and (0.128 g, 0.42 mmol) of FeSO$_4$.7H$_2$O under magnetic stirring (1000 rpm) in closed flask. The aforementioned solution was swiftly supplemented with a new solution of APS (0.17 g, 0.7 mmol) into 50 ml of 0.3 N HCl solution. After one hour of continuous polymerization, Chitosan solution (3 wt % /100 ml, 1 % Acetic acid) was added to the reaction. The polymerization procedure was continuously run for 24 hours at 38°C. The black precipitate was filtered out, repeatedly

_____

rinsed with 0.3 N HCl and distilled water, and subsequently dried at 38°C for a full day to produce the nanopolymeric composites.

3.   Results and discussion

3.1. FTIR Spectra declarations of developed nanopolymeric composites of inhibitors

The FTIR spectra in Fig. 1 display basic band in the scale 1091–1098 cm^{-1} corresponding to the stretch vibrating of characteristic C–O–C functional group of chitosan. This band indicated the good plantation of Chitosan nanoparticles in poly-OAP-co-AA, poly-AA and poly-OAP. The spectrum of CH/poly-OAP-co-AA shows basic band in 1199 cm^{-1} was accompanied to the C-O-H phenolic vibrations of deformation. This absorption demonstrates that the produced copolymer contains an o-aminophenol unit. [18]. Also, it shifts to 1210 cm^{-1} in the spectrum of poly-OAP. In contrast, the bands in 3313 and 1630 cm^{-1} correspond to carboxylic -OH and -COO vibrating groups. This demonstrates that the copolymer chain's -COOH group was added. While these bands appear in poly-AA at 3297 and 1632 cm^{-1}[19]. For all synthesized nanocomposites, the bands that are located nearly at 1518 -1505 cm^{-1} can be attributed to the quinoid ring's C=C vibrations and the benzenoid ring's C=N stretching. Also, peaks at 1204–1244 cm^{-1} are accompanied to the vibrating stretch C-N group of 2° aromatic amine [20-21]. These findings showed the emerald structure for CH/poly-OAP-co-AA, CH/poly-AA and CH/poly-OAP.
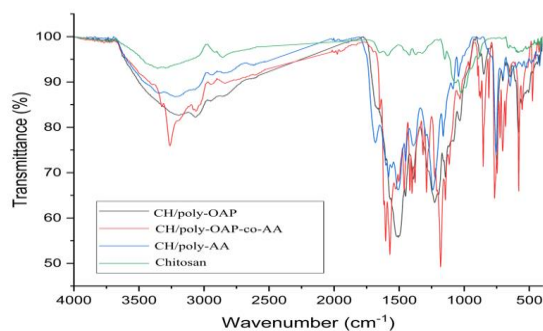

Figure 1: FTIR spectra of CH/poly-OAP-co-AA, CH/poly-AA, CH/poly-OAP & Chitosan.

3.2.   Electronic   chemical   analyses (Potentiodynamic polarisation)

mild steels into 0.1 M HCl potentiodynamic polarisation curves in the absence and presence of various concentration polymers are shown in Fig. 2. Inhibition efficiency (%IE), cathodic (βc) Tafel slopes, anodic (βa) Tafel slopes, corrosion (I$_{corr}$) current density, and corrosion (E$_{corr}$) potential were

the potentiodynamic polarisation parameters investigated.
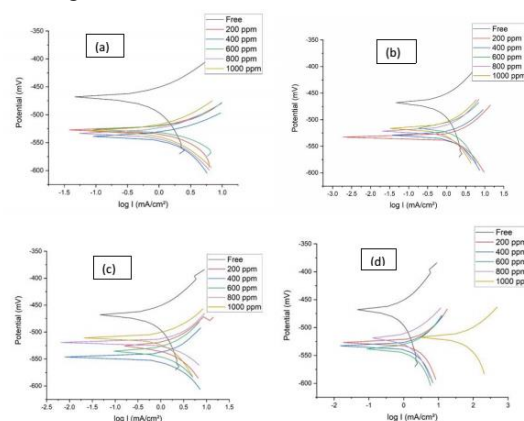

Figure 2: Anodic and cathodic polarisation patterns of a steel electrode in aqueous solutions of 0.1 M HCl containing various amounts of (a) CH/poly-OAP-co-AA, (b) CH/poly-AA, (c) CH/poly-OAP & (d) Chitosan at 25°C.

The subsequent equation had been employed to determine the inhibitory effectiveness [22]:

$$IE\% = (1 - (I_{inh}/I_{free})) * 100$$

Where I$_{inh}$ and I$_{free}$, respectively, represent the corrosion currents of steel electrodes in the presence and absence of inhibitory molecules. In Table 2, the IE% rises as inhibitory particles' concentration increases.

3.3. Adsorption Isotherm

The subsequent equation had been employed to count how much of the steel surface is covered by substances that have been adsorbed onto it [22].

$$\theta = 1 - (I_{inh}/I_{free})$$

It has been discovered that when additive concentrations rise, so does surface coverage. In Fig. 3, Straight lines with constant slopes result from plotting (C/θ) versus inhibitor concentration (C). This suggests that the adsorption of inhibitory species is observed by Langmuir adsorption isotherm.
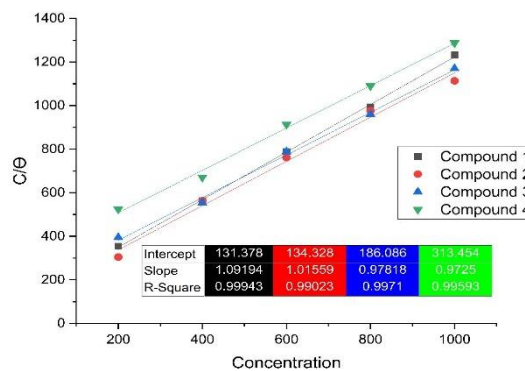

Figure 3: Adsorption isotherm of Langmuir for the adsorption of CH/poly-OAP-co-AA, CH/poly-AA,

_____

CH/poly-OAP & Chitosan of the mild steel in 0.1 M HCl at 25°C.

3.4. Effect of temperature

In a 0.1 M HCl solution with 1000 ppm of inhibitors, the influence of heat on corrosion measurements like E_{corr}, IE% and I_{corr} was investigated over various degrees of temperature of 25-65 °C. The findings demonstrated that temperature change had essentially little impact on the polarisation curves' shapes. The information in Table 3 demonstrated that while I_{corr} values increased as temperature rose, E_{corr} values switched to fewer negative levels. This shows how the corrosion reaction is accelerated by increased temperature. However, when the temperature rises, the effectiveness of the inhibition reduces. This is a result of temperature increases speeding up the desorption process.

The formula devised by Arrhenius is employed to estimate the rate of corrosion reaction [22].

$$\log(I_{corr}) = \log(A) - E_a/2.303RT$$

Where the rate of the corrosion response is represented by I_{corr}, E_a is the corrosion reaction's activation energy, R is ideal gas constant (8.314 $J \cdot K^{-1} \cdot mol^{-1}$), T is absolute temperature, and A is the Arrhenius factor.

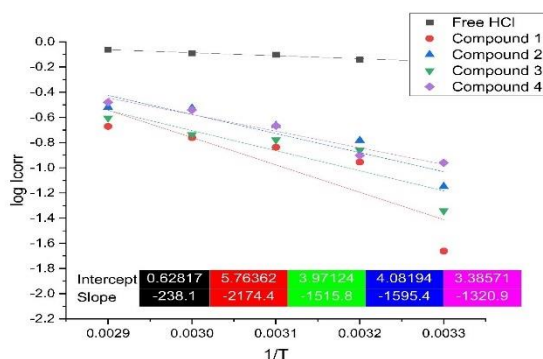The log (Icorr) against (1/T) plot resulted in the straight lines shown in the following figure.

Figure 4: The association between log (I_{corr}) and 1/T of steel electrode in 0.1 M HCl, in either the absence or the presence of 1000 ppm of various inhibitors.

The transition state model was used to derive the additional activation thermodynamic parameters ΔH^*, ΔS^* [22];

$$\log(\frac{Icorr}{T}) = (\log\left(\frac{R}{hn}\right) + (\frac{\Delta S*}{2.303\ R}) - (\frac{\Delta H*}{2.303\ RT})$$

Where R is the ideal gas constant (8.314 J/mol.k), n is Avogadro's number (6.02×10^{23}), and h is the plank

constant (6.62×10^{-34} m² kg/s), respectively, and where ΔS^* and ΔH^* are the entropy and the enthalpy change, graphing log (I_{corr}/T) vs (1/T) results in straight lines in the next figure.
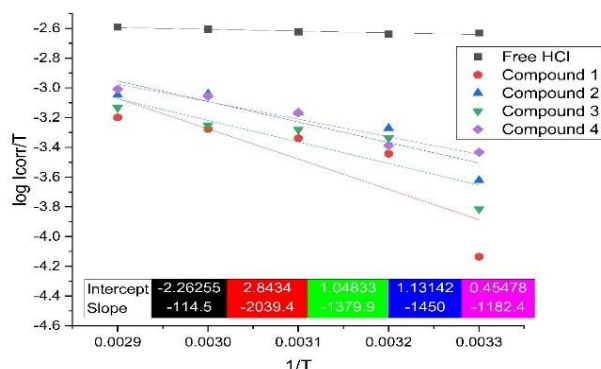

Figure 5: The relationship between log (I_{corr}/T) and 1/T for steel electrode in 0.1M HCl in the absence and presence of 1000 ppm of various inhibitors

Table (4) contains the values of ΔH^* and ΔS^* that were determined by plotting log (I_{corr}/T) vs (1/T) straight lines with a slope of $(-\Delta H^*)/(2.303R)$ and an intercept of (log (R/nh)) + ($(\Delta S^*)/(2.303\ R)$). At 298 K, the renowned equation may be used to determine the variation in the activation free energy (ΔG^*) of the corrosion process [22].

$$\Delta G^* = \Delta H^* - T\Delta S^*$$

In Table (4), the derived ΔG^* values are also reported.

It is evident that the presence of the inhibitor causes an increase in activation energy, and that this is due to the inhibitor's adsorption on the surface of the metal.

The mechanism of corrosion is an endothermic one, as shown by the positive sign of ΔH^*, and the raised measurements of E_a that are analogous to the values of ΔH^* hint that the corrosion process is gaseous, which can be readily understood by the generation of hydrogen gas along with the reduction in reaction volume [22].

The decline in freedom of the mechanism is shown by the negative values of entropy (ΔS^*), which are related to a rise in order and the creation of metal-nanocomposites complexes. Table (5) compares the modified Chitosan's highest inhibitory effectiveness (IE%) with the findings of the current investigation [23-27].

Table 1: Mild steel chemical constitution.

Substance	Fe	Mn	S	Ni	P	Si	Cr	C
Wt %	rest	0.495	0.157	0.006	0.060	0.157	0.047	0.158

Table 2: Steel electrode corrosion characteristics in 0.1 M HCl solution at various inhibitor doses.

medium	Conc.(ppm)	βa	-βc	-E$_{corr}$	I$_{corr}$	IE%
Free HCl		92.000	109.30	524.00	0.6975	0.000
CH/poly-OAP-co-AA (Comp.1)	200.00	93.000	98.200	530.00	0.4850	56.32
	400.00	78.200	100.20	513.90	0.2025	70.96
	600.00	101.60	90.800	529.50	0.1667	76.10
	800.00	87.600	106.70	520.00	0.1156	83.40
	1000.0	103.00	111.00	503.00	0.0218	96.87
CH/poly-AA (Comp. 2)	200.00	94.800	124.20	536.30	0.2395	65.67
	400.00	100.20	115.30	532.00	0.2019	71.05
	600.00	72.900	100.90	521.80	0.1477	78.82
	800.00	74.000	101.30	522.80	0.1258	81.96
	1000.0	67.900	105.40	519.00	0.0711	89.80
CH/poly-OAP (Comp. 3)	200.00	95.600	97.000	524.70	0.3439	50.70
	400.00	104.30	120.00	510.90	0.1932	72.30
	600.00	95.100	115.00	500,00	0.1787	74.37
	800.00	113.00	130.00	504.00	0.1355	80.57
	1000.0	97.800	119.00	490.00	0.0456	93.40
Chitosan (Comp. 4)	200.00	101.00	119.50	531.00	0.4313	38.16
	400.00	85.600	97.600	517.00	0.2814	59.65
	600.00	83.200	104.70	524.00	0.2392	65.70
	800.00	98.000	109.70	519.40	0.1855	73.40
	1000.0	82.700	95.800	522.70	0.1098	84.25

Table 3: impact of temperature on the corrosion variables of steel electrode in 0.1 M HCl and 0.1 M HCl with 1000ppm of various inhibitors.

Compound	T(K)	-E$_{corr}$	I$_{corr}$	IE%
HCl 0.1 M	298	529.70	0.6975	0.000
	308	540.00	0.7245	0.000
	318	529.80	0.7919	0.000
	328	531.00	0.8135	0.000
	338	526.80	0.8658	0.000
CH/poly-OAP-co-AA (Comp.1)	298	502.00	0.0218	96.87
	308	505.80	0.1110	84.67
	318	517.60	0.1456	81.61
	328	528.70	0.1733	78.69
	338	532.30	0.2133	75.36
CH/poly-AA (Comp. 2)	298	525.70	0.0711	89.80
	308	522.60	0.1648	77.25
	318	533.60	0.2173	72.55
	328	528.70	0.2782	65.80
	338	521.60	0.3031	64.99
CH/poly-OAP (Comp. 3)	298	506.40	0.0456	93.40
	308	513.70	0.1412	80.50
	318	528.20	0.1669	78.90
	328	505.00	0.1834	77.45
	338	507.00	0.2484	71.30
Chitosan (Comp. 4)	298	519.70	0.1098	84.25
	308	516.50	0.1255	82.67
	318	509.90	0.2162	72.69
	328	524.20	0.3081	62.12
	338	502.70	0.3616	58.23

_____

Table 4: Activation thermodynamic parameters of the steel electrode's dissolving process in 0.1 M HCl solution, both in the absence and presence of 1000 ppm of various inhibitors at 298K.

Compound	E_a KJ/mol.k	ΔH^* KJ/mol.k	$-\Delta S^*$ KJ/mol.k	ΔG^* KJ/mol.K
HCl 0.1 M	4.558	2.192	0.241	74.01
CH/poly-OAP-co-AA (Comp.1)	41.633	39.048	0.143	81.662
CH/poly-AA (Comp. 2)	29.023	26.421	0.177	79.167
CH/poly-OAP (Comp. 3)	30.547	27.763	0.175	80.172
Chitosan (Comp. 4)	25.291	22.639	0.188	78.922

Table5: Comparison of maximum inhibitory efficiency (IE%) for modified Chitosan with present study.

Compound	IE%	References
CHC and CAHC	87.97 and 93.95	[23]
SLC	96.44	[24]
GO-CS and GO-CS-ZnO	83.81 and 85.61	[25]
CH-HQ	93	[26]
CH-ZnO NPs	93.95	[27]
CH/poly-OAP-co-AA	96.87	Present work
CH/poly-AA	89.80	Present work
CH/poly-OAP	93.40	Present work

3.5. Surface Investigation

Fig.6a & 6b display SEM and TEM images of the surface of a new synthesized nanocomposite inhibitor CH/poly-OAP-co-AA. To ascertain the dispersion of the Chitosan nanoparticles via poly-OAP-co-AA, the SEM images in Figure 6a were examined. The Chitosan nanoparticles were equally dispersed throughout the copolymer, according to the pictures shown here. TEM methods, as seen in Figure 6b validated the nanocomposite's CH/poly-OAP-co-AA core-shell structure.

Fig. 7a & 7b display SEM images of the surface of mild steel soaking in 100 mL of HCl 0.1 M in the absence and presence of 1000 ppm of CH/poly-OAP-co-AA for 72-hour, respectively. The surface of the steel is significantly exposure to hydrochloric acid causes the metal to oxidize, leaving away tiny voids. However, this corrosive effect has lessened in the presence of the inhibitor, which is the result of the inhibitor molecule creating a protective barrier on the metal surface [11].
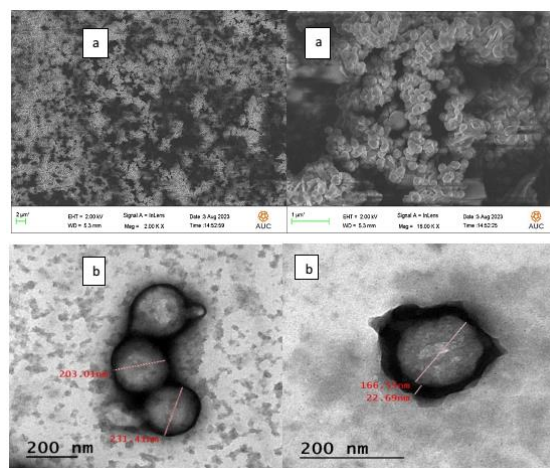

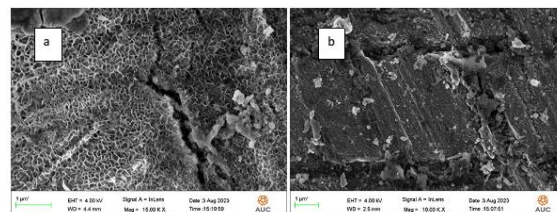Figure 6: (a) SEM and (b) TEM images of CH/poly-OAP-co-AA

Figure 7: SEM images of the surface of mild steel soaking in 100 mL of HCl 0.1 M in (a) the absence and (b) presence of 1000 ppm of CH/poly-OAP-co-AA for 72-hour.

_____

4. Conclusion

By combining nano particles of Chitosan within presence the copolymerization of Anthranilic acid and o-Aminophenol, core-shell nanocomposite CH/poly-OAP-co-AA was effectively created. Utilizing FTIR, TEM and SEM it was investigated. Electrochemical studies were used to examine it as a stainless steel corrosion preventative in an acidic medium. These are the outcomes: (1) The combined interactions of copolymeric modified chitosan core-shell nanocomposite result in a higher corrosion inhibition effectiveness for CH/poly-OAP-co-AA (96.87%) than for CH/poly-OAP (93.40%), CH/poly-AA (89.80%) and Chitosan (84.25%). (2) Tafel curves show that when inhibitor concentration rose in the corrosive medium inhibitory efficiency (IE%) increased and Icorr, the corrosion current density, dropped. (3) The adsorption of CH/poly-OAP-co-AA on the surface of mild steel complies with the Langmuir isotherm, acting as a mixed type inhibitor. (4) Surface examination of mild steel in both the presence and absence of an inhibitor revealed that CH/poly-OAP-co-AA may effectively adsorb to the surface of the steel to stop corrosion. In conclusion, the utilisation of copolymeric modified chitosan core-shell nanocomposite can enhance the anticorrosion strengths of these compounds as a green inhibitor. Also, cheap preparation is a useful strategy for preventing corrosion in the sector.

References

1- Desai, P.D., Pawar, C. B., Avhad, M. S., and More, A. P. *Corrosion inhibitors for carbon steel: A review.* Vietnam Journal of chemistry, 2023.61: p. 15-42.

2-Hebbar, N., Praveen, B. M., Prasanna, B. M., Venkatesha, T. V., and Abd Hamid, S. B. *Anthranilic Acid as Corrosion Inhibitor for Mild Steel in Hydrochloric Acid Media.* Journal of Procedia Material Science, 2014. 5: p.712–718.

3- Shirazi, Z., Golikand, A. and Keshavarz, M. A new nanocomposite based on poly (o-anthranilic acid), graphene oxide and functionalized carbon nanotube as an efficient corrosion inhibitor for stainless steel in severe environmental corrosion. Journal of Composite Communication, 2020. 22: p. 100467.

4- Suma, N. D., Corrosion Inhibition and Adsorption Characteristics of N-Phenyl Anthranilic acid on Mild steel in Acid medium. Journal of Materials Today: Proceedings, 2020. 24: p. 2424-2428.

5- Yahaya, S. M., Harun, M. K., and Ismail, I. *Corrosion Inhibition of Mild Steel by Electrodeposited Poly(M-Aminophenol) coating.* Journal of Solid State Phenomena,2021. 317: p. 498-505.

6- Ciriello, R., Carbone, M.E., Coviello, D., Guerrieri, A., and Salvi, A.M. Improved stability of thin insulating poly(o-aminophenol) films in aqueous solutions through an efficient strategy for electrosynthesis under neutral pH conditions: Electrochemical and XPS investigation. Journal of Electroanalytical Chemistry, 2020. 867: p. 114183.

7- Verma, C., Quraishi, M.A., Alfantazi, A., and Rhee, K. *Corrosion inhibition potential of chitosan based Schiff bases: Design, performance and applications.* International Journal of Biological Macromolecules, 2021. 184: p. 135-143.

8- Lai, X., Hu, J., Ruan, T., Zhou, J., and Qu, J. Chitosan derivative corrosion inhibitor for aluminum alloy in sodium chloride solution: A green organic/inorganic hybrid. Journal of Carbohydrate Polymers, 2021. 265: p. 118074.

9- Zhao, Q., Guo, J., Cui, G., Han, T. and Wu, Y. *Chitosan derivatives as green corrosion inhibitors for P110 steel in a carbon dioxide environment.* Journal of Colloids and Surfaces B: Biointerfaces, 2020. 194: p. 111150.

10-Ansari, K.R., Chauhan, D. S., and Quraishi, M.A. *Chitosan Schiff base: an environmentally benign biological macromolecule as a new corrosion inhibitor for oil & gas industries.* International Journal of Biological Macromolecules, 2020. 144: p. 305-315.

11- Hepziba, S.J., Jessima, M., Berisha, A., and Srikandan, S. Preparation, characterization, and evaluation of corrosion inhibition efficiency of sodium lauryl sulfate modified chitosan for mild steel in the acid pickling process. Journal of Molecular Liquids, 2020. 320: p. 114382.

12- Badr, E., Hassan, H. H., and Shafek, H. Synthesis of anionic chitosan surfactant and application in silver nanoparticles preparation and corrosion inhibition of steel. International Journal of Biological Macromolecules, 2020. 157: p. 187-201.

13- Benhib, F., and Hssisou, R. Green synthesis of novel carbohydrate polymer chitosan oligosaccharide grafted on d-glucose derivative

as bio-based corrosion inhibitor. Journal of Molecular Liquids, 2021. 322: p. 114549.

14- Chauhan, D. S., EL Mouaden, K., Quraishi, M. A., and Bazzi, L. Aminotriazolethiol-functionalized chitosan as a macromolecule-based bioinspired corrosion inhibitor for surface protection of stainless steel in 3.5% NaCl. International Journal of Biological Macromolecules, 2020. 152: p. 234-241.

15- Akinbulumo, O. A., Odejobi, O. J., and Odekanle, b. Thermodynamics and adsorption study of the corrosion inhibition of mild steel by Euphorbia heterophylla L. extract in 1.5 M HCl. Journal of Results in Materials, 2020. 5: p. 100074.

16- Baach, B., and Ferraa, S. Experimental evaluation of new inorganic compounds based on bismuth oxide Bi$_2$O$_3$ as corrosion inhibition for mild steel in acidic medium. Journal of Inorganic Chemistry Communications, 2022. 137: p. 109233.

17- Das, S., Singh, V. K., and Dwivedy, A.K. Encapsulation in chitosan-based nanomatrix as an efficient green technology to boost the antimicrobial, antioxidant and in situ efficacy of Coriandrum sativum essential oil. International Journal of Biological Macromolecules, 2019. 133: p. 294-305.

18- Ghonem, M. A., and El-Enany, G. *Development of conducting poly(o-amino phenol) film and its capacitance behaviour.* International Journal of Electrochemical Science, 2016. 11: p. 9987–9997.

19- Zoromba, M. Sh., Tashkandi M. A., and Alshehri A. A. *Polymer solar cell based on doped o-anthranilic acid and o-aminophenol copolymer.* Journal of Optical Materials, 2020. 104 : p. 109947.

20. Yakuphanoglu, F., Basaran, E., Senkal, B. F., Sezer, E. Electrical and optical properties of an organic semiconductor based on polyaniline prepared by emulsion polymerization and fabrication of Ag/polyaniline/n-SiSchottkydiode. Journal of Physical Chemistery B, 2006. 110: p.16908–16913.

21. Quillard, S., Louarn, G., Buisson, and J. P. *Vibrational spectroscopic studies of the isotope effects in polyaniline.* Journal of Synthetic Metal, 1997. 84: p. 805–806.

22. ElDesouky, M. M., Eldougdoug, W. I., Fouad, E., and Abd El-Moneim, M. *The synthesis of new corrosion inhibitors based on modified chitosan to provide protection over mild steel.*

Egyptian Journal of Chemistry, 2023. doi: 10.21608/ejchem.2022.127782.5668.

23. Zhao, Q., Guo, J., and Cui, G. *Chitosan derivatives as green corrosion inhibitors for P110 steel in a carbon dioxide environment.* Colloids and Surfaces B: Biointerfaces, 2020. 194: p. 111150.

24. Hepziba, S. J., and Subhashini, S. Preparation, characterization, and evaluation of corrosion inhibition efficiency of sodium lauryl sulfate modified chitosan for mild steel in the acid pickling process. Journal of Molecular Liquids, 2020. 320, Part A: p. 114382.

25. Majidi, H., and Mirzaee, A. Fabrication and characterization of graphene oxide-chitosan-zinc oxide ternary nano-hybrids for the corrosion inhibition of mild steel. International Journal of Biological Macromolecules, 2020. 148: p. 1190-1200.

26. Rbaa, M., and Fardioui, M. 8-Hydroxyquinoline based chitosan derived carbohydrate polymer as biodegradable and sustainable acid corrosion inhibitor for mild steel: Experimental and computational analyses. International Journal of Biological Macromolecules, 2020. 155: p. 645-655.

27. Hasanin, M., and & Al Kiey, sh. Development of ecofriendly high performance anti-corrosive chitosan nanocomposite material for mild steel corrosion in acid medium. Biomass Conversion and Biorefinery, 2021. 13: p. 12235–12248.